Generating long-term sub-hourly wind speed time series by coupling mesoscale models with full-scale spectra

Generating long-term sub-hourly wind speed time series by coupling mesoscale models with full-scale spectra

David Schillebeeckx[1] **and Grégoire Leroy**[1]

[1] 3E nv, Kalkkaai 6, 1000 Brussels, Belgium

E-mail: david.schillebeeckx@3e.eu

Abstract. Time series-based wind studies are gaining more and more interest and importance within the wind resource community. Benefits of such time series-based analysis being, among others, more accurate production and loss estimations, better representation of ramp-up and extreme events, and improvements in the dimensioning of energy storage systems. While mesoscale Numerical Weather Prediction (NWP) models can simulate long-term winds that capture non-stationary weather patterns, it is known that they are not able to properly resolve sub-scale processes leading to a smoothing effect. Recent studies presented spectral models that describe the full atmospheric spectrum of boundary layer winds which connect the microscale turbulent movements to the large, mesoscale fluctuations. In this work, mesoscale simulations from the Weather Research and Forecasting (WRF) model are coupled with stochastic turbulence simulations using state-of-the-art full-scale boundary-layer spectra to efficiently bridge the spectral gap between the mesoscale and the turbulence fluctuations, without requiring any local measurements nor expensive CFD simulations. The study provides a practical step-by-step approach to generate long wind speed time series at high sampling rate at any desired location and height.

1. Introduction

As an atmospheric quantity, wind speed is naturally volatile and spatiotemporal fluctuations occur at a wide range of scales from planetary and annual variations down to the turbulent scale. For wind energy yield assessments, these wind variations have historically been represented through statistics and histograms [1]. However, with the increase of computational power, wind energy production estimates are more and more being calculated directly in the time domain. The use of time series typically lowers the uncertainty as it avoids imposing Weibull distributions that introduce fitting errors [2]. Additionally, time series include the atmospheric seasonal and diurnal variations into the production estimations, hereby also introducing the varying atmospheric quantities such as stability, air density, turbulence and wind shear into the calculations allowing to correctly model their influence on the turbines performance and turbine interaction effects. Time series-based calculations also enable to estimate complex time-dependent losses and the interaction and overlap between them more accurately. These include for example losses due to bat and bird protection stops, noise reduction operations modes, grid export limitations, shadow flicker curtailments, etc. Consequently, the combination of these benefits of time series-based energy yield assessments allows to lower the uncertainty on the

long-term production estimation. Additionally, for turbine load assessments, high-frequency wind data down to the turbulent scale are imperative to capture the dynamic effects of the turbine and estimate the components fatigue life [3]. Furthermore, the increasing share of intermittent wind power plants in the energy production mix also calls for wind generation time series with a high temporal resolution. For high penetration of wind in the power system, sub-hourly production data for wind integration studies are required to correctly capture the load variability, start-ups and ramp effects [4]. High resolution time series are also crucial for complex wind and storage systems, as the time resolution of the data can significantly impact the dimensioning and investment decision of storage systems [5]. Lastly, from a financial point of view, balancing of the consumption and production profiles is becoming more challenging with volatile electricity prices and complex hybrid plants combining different production and storage technologies.

Numerical Weather Prediction (NWP) models, such as the mesoscale Weather Research and Forecasting (WRF) model, and reanalysis products can provide long-term wind time series based on historical weather data that are proven to be a reliable source for wind energy assessment studies [6, 7, 8]. Although numerical simulations show great performances for the estimation of the mean wind regime over large areas, the models are constrained by their spatial and temporal resolution limits. The terrain is represented by a relatively coarse grid with a resolution of a few kilometres and therefore does not allow to capture the smaller sub-grid phenomena, such as topographic speed-up effects [9]. Furthermore, because of the filtering and dampening numerical schemes in mesoscale models, the effective temporal resolution is further reduced [10]. These limitations of the effective model resolution lead to a smoothing effect of the wind and therefore to a reduced wind variability [9, 11]. The spatial and temporal averaging of mesoscale simulations result in low-resolution, e.g. hourly, wind time series that do not capture the actual microscale fluctuations and turbulence on site. Downscaling these low-resolution wind simulations using high fidelity Computational Fluid Dynamics (CFD) models is possible but comes at a high computational cost [12]. While more cost-efficient methods exist to spatially downscale mesoscale simulations and correcting for the coarse topographic representation such as the WRF-WAsP method in [13], efficient alternatives for a temporal downscaling, going from hourly to a higher temporal resolution, are lacking. The CorRES tool [14] introduces sub-hourly variations to hourly WRF simulations with stochastic model that simulates high frequency fluctuations from a power spectrum density (PSD) function. However, similar as in the Spectral Correction Method (SCM) from [9, 11], the spectrum for higher frequencies is extended following $S(f) \propto f^{-5/3}$ which is only valid for lower frequencies and therefore limits its applicability to model fluctuations up to $\sim 10\,\text{min}$. Recent studies present full-scale boundary layer spectra that cover the mesoscale atmospheric motions down to the fast fluctuations of the boundary layer turbulence [15, 16]. Therefore, these spectral models enable to simulate wind speed fluctuations for a higher frequency and generate realistic turbulence that can be added to the mesoscale time series.

This paper presents such a hybrid approach by coupling mesoscale wind speed with stochastic turbulence simulations based on full-scale boundary layer models. Similar principles were applied as in [17], where measurements with a 10 min resolution were used to capture the non-stationary wind speed characteristics instead of NWP simulations. The authors also mention the possibility of using mesoscale simulations as an alternative for measurements but address the limitation of effective time resolution of such models. This work addresses this issue by first applying a correction on the mesoscale fluctuations in a similar fashion as the SCM but directly on the spectral components rather than on the spectral moments to allow for a time series analysis (subsection 3.1). Then, physically realistic turbulence at any desired sampling are generated by building upon the advancements in the boundary layer spectral models from [15] and [16] (subsection 3.1). The combination of these modelled low- and high-frequency spectra covers

the full boundary-layer spectrum and thus closes the spectral gap between the meso- and microscale (subsection 3.2). The methodology has been validated against observations in section 4. The mesoscale and measurement data used are briefly discussed in the following section and conclusions are drawn in section 5.

2. Data and background

To demonstrate the different steps of the methodology outlined in this paper, WRF simulations are used for the mesoscale input data. Similar model setup and parameterisations were used as in the New European Wind Atlas (NEWA) production run [8], but with an hourly output time step instead of half-hourly. Although WRF has been used for the purpose of showcasing the applied techniques, the methodology outlined here is generic and is suited for simulations from other NWP models or for reanalysis datasets as well.

As a reference, and for validation, measurements from a 30 m meteorological mast within the WRF domain were used. The measurements consist of 1-year of wind speed data from a cup anemometer with a recording frequency of 1 Hz. The site is land-based with a flat terrain, however, it can be considered as complex in term of roughness due to the presence of multiple industrial buildings an forest patches around the mast. Wind speed data has then been extracted from the closest grid point of the WRF simulation.

The reader should note that since the power spectra can appear relatively noisy at higher frequencies, logarithmic smoothing is often applied to remove this noise and highlight the shape of the spectrum.

3. Methodology

Mesoscale simulations show great performances in simulating wind speed time series that capture the non-stationarity of long-term variations. However, these simulations have two shortcomings as discussed in the introduction:

(i) the modelled spectrum underestimates the spectral energy level in the mesoscale range because of the dampening effect in the mesoscale simulations; and

(ii) the limited output time resolution of the simulations (typically hourly) do not capture the higher frequency fluctuations in the microscale range.

These two limitations of the mesoscale simulations will be tackled in three main steps. First, the dampening effect of the mesoscale simulations is alleviated by using the Larsén mesoscale spectral model [18] and correcting the modelled mesoscale time series in the frequency domain. As a next step, the low-resolution time series are temporally downscaled by adding physically realistic turbulence fluctuations using a recent full-scale spectral model [15, 16]. Finally, the resulting spectrum can be converted to the time domain with a Fourier transform to obtain high-frequency wind speed time series for any desired output resolution dt. This high frequency data can further be resampled to arrive at 10-minute mean and standard deviation wind speed values that mimics field observations in a realistic manner.

These steps are discussed in more detail in the following subsections.

3.1. Mesoscale spectral correction

As a first step, the smoothening effect by the WRF simulations that leads to an underestimation of the hourly wind variability will be corrected. The correction will be applied in the frequency domain and follows similar principles as the Spectral Correction Method (SCM) described in [9, 11].

The mesoscale wind behaviour can be represented with the Larsén mesoscale spectrum derived in [18]. This spectral model is applicable for the large-scale mesoscale wind fluctuations in the lower frequency range from approximately 10^{-6} Hz to 10^{-3} Hz:

$$S_{\text{Larsén}}(f) = a_1 f^{-5/3} + a_2 f^{-3}, \tag{1}$$

where the values of the two coefficients, $a_1 = 3 \times 10^{-4}\,\text{m}^2\,\text{s}^{-8/3}$ and $a_2 = 3 \times 10^{-11}\,\text{m}^2\,\text{s}^{-4}$, were obtained from fitting of the model to multiple measurements. To ensure that the spectral model matches the large-scale wind variability at the site, the Larsén mesoscale spectrum is calibrated to the specific site conditions to:

$$S_{\text{meso}}(f) = A \times S_{\text{Larsén}}(f). \tag{2}$$

The calibration coefficient A is obtained through regression from the observed mesoscale spectrum in the frequency range from $8 \times 10^{-6}\,\text{Hz}$ to $3 \times 10^{-5}\,\text{Hz}$, where it is assumed that the WRF simulations are correctly capturing the spectral energy content.

The spectral correction is applied by scaling the WRF simulated spectral energy to the mesoscale spectral model of equation (2) for frequencies above a certain correction frequency f_c. Here, the best results were obtained by selecting $f_c = 2 \times 10^{-5}\,\text{Hz} \approx 1.7\,\text{d}^{-1}$, which is in line with the values reported in [9]. The correction is obtained by first applying a loglinear regression to the observed WRF spectrum:

$$S_{\text{linear}}(f \geq g_c) = b_1 f^{b_2}. \tag{3}$$

The ratio between this linear fit and the calibrated mesoscale spectral model of equation (2) then determines the scaling factor that will be applied to the WRF spectral components at each frequency while keeping the original WRF spectrum untouched for $f < f_c$:

$$S_{\text{WRF,corr}}(f) = \begin{cases} S_{\text{WRF}}(f) & f < f_c \\ S_{\text{WRF}}(f) \times \dfrac{S_{\text{meso}}(f)}{S_{\text{linear}}(f)} & f \geq f_c \end{cases} \tag{4}$$

As an example, and to visually represent the mesoscale correction, Figure 1 shows the WRF spectrum before (a) and after (b) the correction of equation (4) is performed. This correction effectively introduces higher wind variability to the original WRF simulations.

3.2. Microscale spectrum extension

The next step is to include the contribution of the sub-hourly turbulence effects to arrive at any desired output resolution dt ($= 1/f_{\text{output}}$). To simulate these microscale wind speed fluctuations in the high frequency range, the Mikkelsen-Tchen microscale boundary-layer spectral model as described in [19] has been considered. The two-sided representation of this model is:

$$S_{\text{Mikkelsen}}(f) = \frac{a u_*^2 n/n_l}{2f(1 + n/n_l)(1 + n/n_u)^{2/3}}, \tag{5}$$

where $n = fz/U$ is the normalized frequency at height z, u_* the friction velocity, $n_l = f_{\text{Cor}} z/0.6u_*$, $a = 0.953$ and $n_u = 0.185$.

To ensure a smooth transition between the meso- and the microscale, a full-scale boundary-layer spectrum model is required. For this, the approach developed in [15] and applied in [16] to superimpose the meso- and microscale spectral contributions is used:

$$S_{\text{meso+micro}}(f) = \text{equation (2)} + \text{equation (5)} = S_{\text{meso}}(f) + S_{\text{Mikkelsen}}(f). \tag{6}$$

The Fourier coefficients for the high frequency range are then generated from equation (6) using random phase angles following a similar methodology as described in previous studies

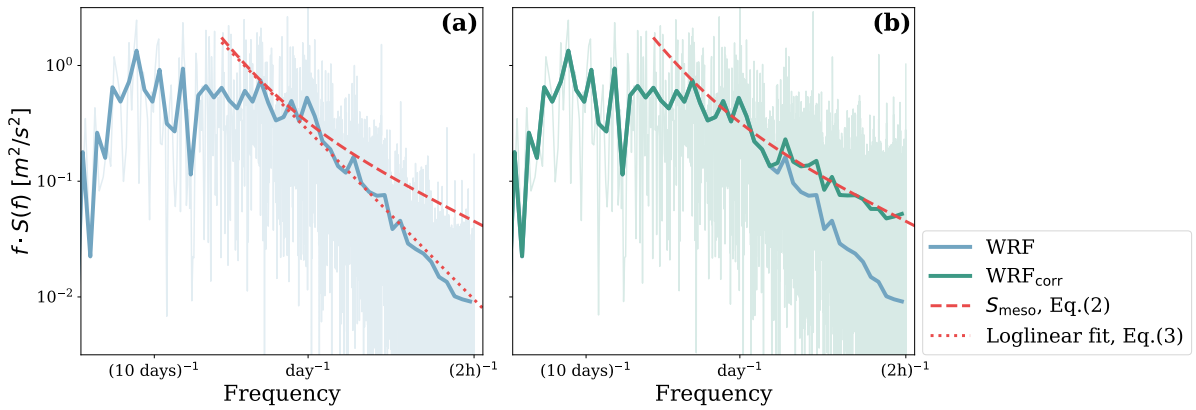

Figure 1. WRF spectra before (a) and after (b) spectral correction. The original WRF spectrum is shown in blue ("WRF") and the spectrum after correction in green ("WRF$_{corr}$"). To visualize the correction applied, the fitted spectral models of equations (2) and (3) are shown as dashed and dotted lines, respectively.

[20, 21]. The generation of the microscale wind fluctuations starts from a list of randomly generated complex numbers with mean 0 and unit variance. Then, the spectral values for each frequency, $S_{\text{meso+micro}}(f)$ from equation (6) are imposed to ensure that the Fourier transform will generate wind speed time series that are coherent with this spectrum.

Following the Nyquist-Shannon sampling theorem, the maximum resolved frequency by the mesoscale simulations is $f_{\text{Nyq,input}} = f_{s_{\text{input,WRF}}}/2 = 1/(2T_{\text{input,WRF}})$. Therefore, high frequency spectral components need to be generated from $f_{s_{\text{input,WRF}}}/2$ to the desired output frequency $f_{\text{output}}/2$ to close the gap with the low-frequency mesoscale simulations. These stochastic simulations are then performed in blocks of length $2T_{\text{input, WRF}}$. For each block the average WRF wind speed, $\bar{U}_{\text{WRF}}$, and friction velocity, $\bar{u}_{*\text{WRF}}$, is calculated as input for the spectral model of equation (6). For the friction velocity, $\bar{u}_{*\text{WRF}}$ is first corrected to the microscale using:

$$u_{*\text{micro}} = \bar{u}_{*\text{WRF}} \frac{\log\left(z/z_{0_{\text{WRF}}}\right)}{\log\left(z/z_{0_{\text{micro}}}\right)}, \tag{7}$$

where $z_{0_{\text{WRF}}}$ is the mesoscale roughness from the WRF simulations and the microscale roughness length, $z_{0_{\text{micro}}}$, can be estimated from roughness maps with the "equilibrium surface roughness" approach as defined in [1]. With the inclusion of $\bar{U}_{\text{WRF}}$ and $u_{*\text{micro}}$ in the meso-micro spectral model, the non-stationarities of both quantities are inherently introduced in the microscale stochastic simulations. Finally, the combination of the different $2T_{\text{input,WRF}}$ blocks results in a simulated turbulence spectrum that covers the high frequency range in the frequency domain.

In this study with hourly WRF simulations, the spectrum will be simulated from $(2\,\text{h})^{-1}$ to $(2\,\text{s})^{-1}$ to arrive at wind time series with an output frequency of 1 Hz. An example of this simulated turbulent spectrum together with the meso-boundary-layer spectral model is shown in Figure 2. For representation purposes, the meso-micro spectral model uses the mean wind speed and friction velocity of the WRF simulations. As the spectral model used for microscale simulations is not constant but actually varies depending on the $\bar{U}_{\text{WRF}}$ and $u_{*\text{WRF}}$ of each $2T_{\text{input,WRF}}$ block, there is not a perfect match between the simulated microscale spectrum and the spectral model as shown in Figure 2. Furthermore, the simulated spectrum in grey also shows that there is some remaining energy content in the lower frequency range ($f < (2\,\text{h})^{-1}$). This originates from the 2 h mean wind speed and friction velocity that drive the turbulence

simulations and leak in some energy content from the mesoscale fluctuations.

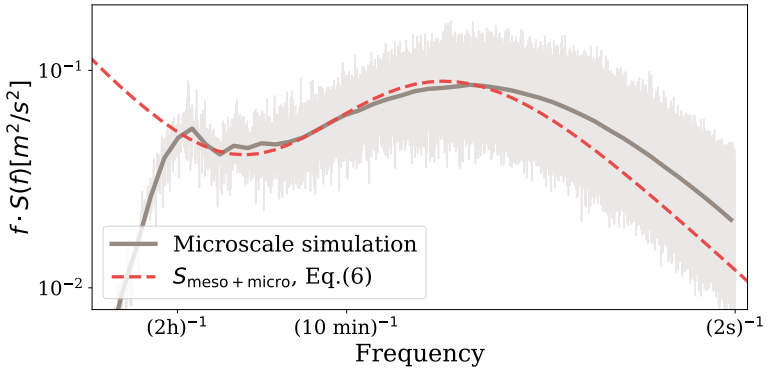

Figure 2. Simulated microscale spectrum to model the high-frequency turbulence fluctuations (grey) together with the meso-boundary-layer spectral model of equation (6) using the mean WRF wind speed and friction velocity (red dashed line).

3.3. Time series generation

For the time series generation, the corrected mesoscale spectrum from equation (4) is joined with the microscale turbulence spectrum from the stochastic simulations as described in subsection 3.2. Here, the corrected WRF simulations will reproduce the long-term non-stationary variations, while the microscale fluctuations in the high-frequency range are covered by the turbulence spectrum. This is visualised in Figure 3. The leakage from the WRF simulations into the microscale spectrum is first removed by a high-pass frequency filter before combining it with the corrected WRF spectrum to ensure a smooth spectrum across all scales.

As a final step, a Fast Fourier Transform (FFT) converts the simulated spectrum from the frequency into the time domain with a time resolution of dt. By grouping the high-resolution time series into 10-minute periods, realistic mean and standard deviation wind speed values can be obtained that resemble the typical output of a meteorological mast from a wind resource measurement campaign.

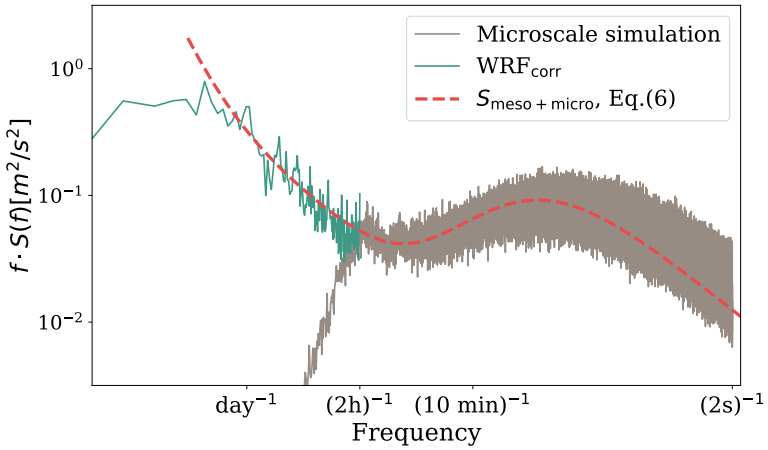

Figure 3. Combination of corrected low-frequency WRF spectrum representing the non-stationary weather patterns (green) with the high-frequency microscale spectrum from stochastic simulations (grey) to capture the turbulence variations. The full meso-micro spectrum used for the simulations is shown as a dashed red line.

4. Results and validation

The final combined $WRF_{corr+micro}$ modelled spectrum is shown together with the measured spectrum in Figure 4. The validation shows a good agreement between the simulated and observed spectrum from the mast measurements throughout the entire spectral domain. This

indicates that the methodology outlined in section 3 is able to generate wind data with physically realistic fluctuations in the mesoscale, gap (the so-called "terra incognita") and microscale regions that resemble actual field observations.

The simulated spectrum can be converted with a FFT to the time domain with a time resolution of 1 second before resampling to 10-minute mean and standard deviation values. Figure 5 shows the first 3 days of high-resolution simulated time series together with the original WRF wind speeds and the observations. The figure shows that the fluctuations of the simulated time series behave in a similar manner as the ones observed from the mast measurements.

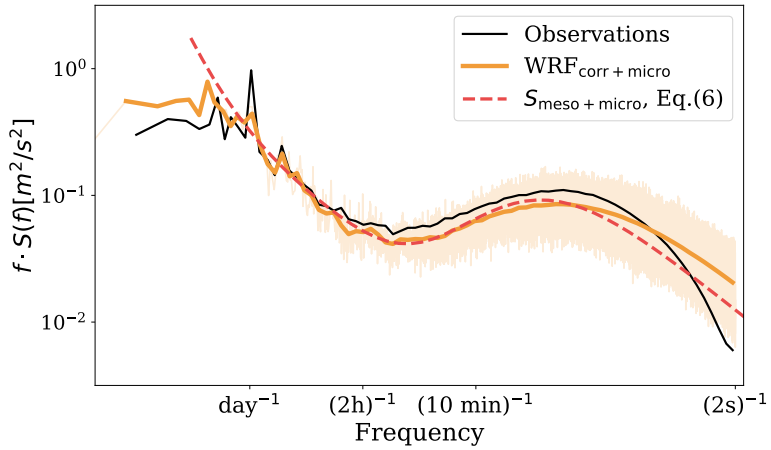

Figure 4. The superposition of the corrected WRF spectrum with the turbulence stochastic simulations (orange) is in good agreement with the observed spectrum (black) throughout the entire boundary-layer spectrum. As a reference, the spectral model used for the simulations is shown as a dashed red line.

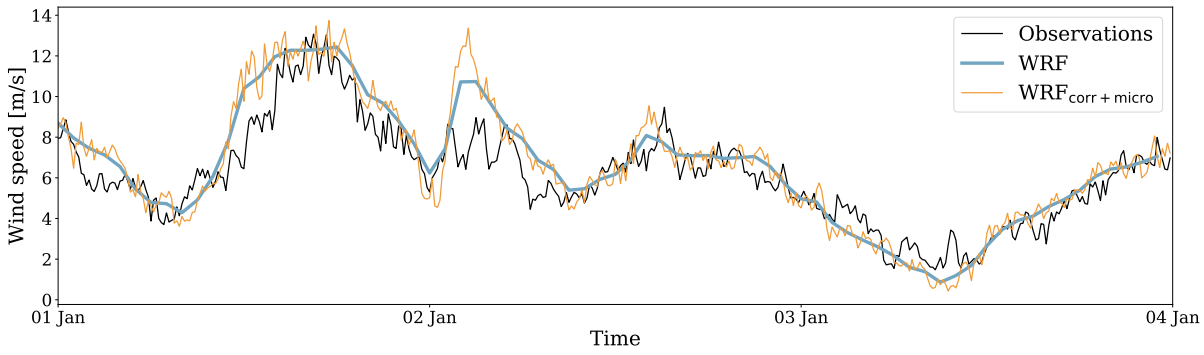

Figure 5. Example of wind speed time series from original hourly WRF simulations (blue), the WRF simulations temporally downscaled to 10 minutes (orange) and the mast measurements (black).

Finally, for wind power integration studies, the ramp behaviour is often investigated [14, 22]. For this, the wind speed ramp amplitude, ΔU, for a predefined time difference, Δt, is calculated:

$$\Delta U_{\Delta t} = U_t - U_{t-\Delta t}. \tag{8}$$

Then, probability and cumulative density functions (PDF and CDF, respectively) for a selected time window can be calculated to verify the ramp rate distribution. Figure 6 shows the PDF and CDF for the 10-minute wind speed differences for both the simulated as measured time series. Although somewhat fatter tails are observed in the measurements, overall, the modelled 10-minute ramps are closely related to the observed ramp distribution. The slight underestimation

of the larger wind speed differences is likely to originate from the assumption of Gaussian distributed turbulence during the stochastic simulations. This deviation from the non-Gaussian nature of atmospheric turbulence can result in an underestimation of the wind turbine extreme and fatigue loads as well [3, 23]. However, as a turbine acts as a low-pass filter, using Gaussian or non-Gaussian turbulence inflow does not necessarily lead to significant differences in the mechanical loads that take time to develop [24]. The relevance of Gaussian versus non-Gaussian turbulence fields on turbine load and fatigue damage therefore still remains an ongoing research discussion.

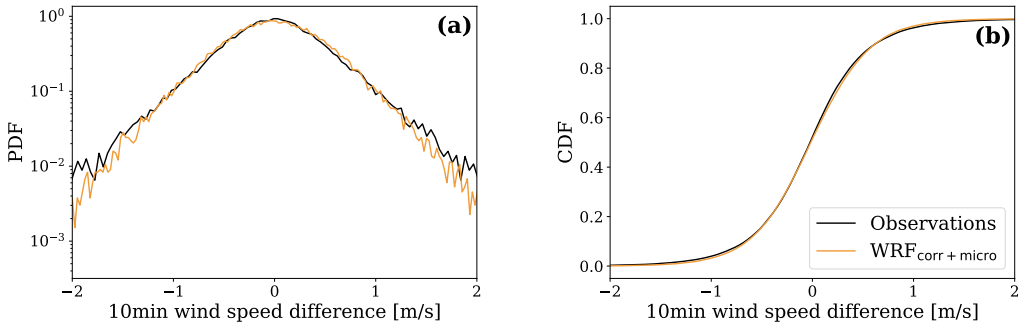

Figure 6. PDF (a) and CDF (b) of the 10-minute ramp rates for the WRF temporally downscaled simulation (orange) compared to the observations (black).

5. Conclusions and outlook

NWP models tend to produce wind speed time series that are excessively smooth and have a limited time resolution. This paper presents a new methodology to temporally downscale mesoscale simulations and generate realistic wind speed data at high temporal resolution without the need for CFD or on-site measurements. This method is demonstrated by coupling mesoscale simulations from the WRF model with stochastic turbulence simulations using a full-scale spectral model to downscale the hourly wind speeds down to 10-minute mean and standard deviation values.

This hybrid approach to couple low-frequency mesoscale time series with high-frequency turbulence simulations can be summarized as follows:

(i) Correct for the smoothing of mesoscale simulations.
  (a) Compute the PSD of the numerical simulations.
  (b) Calibrate the Larsén mesoscale spectrum to observed PSD.
  (c) Correct spectral components to the Larsén mesoscale spectrum model for higher frequencies.

(ii) Extend the mesoscale spectrum to the microscale range.
  (a) Generate microscale spectral components to any desired frequency $1/dt$ using a full-scale boundary layer spectral model.
  (b) Combine the low frequency corrected mesoscale spectrum (i) with the high frequency microscale components (iia).

(iii) Generate time series from the combined modelled spectrum.
  (a) Transform the combined spectrum to time domain with a FFT.
  (b) Resample the high frequency time series to 10-minute mean and standard deviation values to resemble field observations.

The resulting wind speed time series correctly represents non-stationary weather patterns introduced by the mesoscale simulations, as well as the high-frequency turbulent motions captured by the boundary layer spectral models. Using these realistic time series data in wind studies can typically lead to more accurate production and loss estimations. Furthermore, it allows wind experts to improve their assessments of ramping and extreme events or assist in the dimensioning of storage systems.

A more extensive validation is planned to verify the performance of the temporal downscaling methodology at multiple sites with different topographical and atmospheric conditions. Furthermore, the modelling approach can be extended by including the downscaling of the lateral velocity component, v, to reproduce high frequency wind direction variations as well. This can be achieved with the same stochastic simulation principles as discussed in subsection 3.2 together with the latest advancements in the full-scale v spectral model from [21].

Acknowledgements

The work on this paper is part of the WindSider project. It has been carried out with the support of the EU Horizon 2020 call H2020-EIC-FTI-2018-2020 (Agreement n° 878788).

References

[1] Troen I and Lundtang Petersen E 1989 *European Wind Atlas* (Risø National Laboratory) ISBN 87-550-1482-8
[2] Jourdier B and Drobinski P 2017 *Annales Geophysicae* **35** 691–700
[3] Wächter M, Heißelmann H, Hölling M, Morales A, Milan P, Mücke T, Peinke J, Reinke N and Rinn P 2012 *Journal of Turbulence* N26
[4] Deane J, Drayton G and Gallachóir B Ó 2014 *Applied Energy* **113** 152–8
[5] Troy N, Flynn D and O'Malley M 2012 The importance of sub-hourly modeling with a high penetration of wind generation *2012 IEEE Power and Energy Society General Meeting* (IEEE) pp 1–6
[6] Al-Yahyai S, Charabi Y and Gastli A 2010 *Renewable and Sustainable Energy Reviews* **14** 3192–8
[7] Staffell I and Pfenninger S 2016 *Energy* **114** 1224–39
[8] Hahmann A N, Sīle T, Witha B, Davis N N, Dörenkämper M, Ezber Y, García-Bustamante E, González-Rouco J F, Navarro J, Olsen B T *et al.* 2020 *Geoscientific model development* **13** 5053–78
[9] Bastine D, Larsén X, Witha B, Dörenkämper M and Gottschall J 2018 *Journal of Physics: Conference Series* **1102** 012006 URL `https://doi.org/10.1088/1742-6596/1102/1/012006`
[10] Skamarock W C 2004 *Monthly weather review* **132** 3019–32
[11] Larsén X G, Ott S, Badger J, Hahmann A N and Mann J 2012 *Journal of Applied Meteorology and Climatology* **51** 521–33
[12] Rodrigo J S, Arroyo R C, Gancarski P, Guillén F B, Avila M, Barcons J, Folch A, Cavar D, Allaerts D, Meyers J and Dutrieux A 2018 *Journal of Physics: Conference Series* **1037** 072030 URL `https://doi.org/10.1088/1742-6596/1037/7/072030`
[13] Dörenkämper M, Olsen B T, Witha B, Hahmann A N, Davis N N, Barcons J, Ezber Y, García-Bustamante E, González-Rouco J F, Navarro J *et al.* 2020 *Geoscientific model development* **13** 5079–102
[14] Koivisto M, Jónsdóttir G M, Sørensen P, Plakas K and Cutululis N 2020 *Renewable Energy* **159** 991–9
[15] Larsén X G, Larsen S E and Petersen E L 2016 *Boundary-layer meteorology* **159** 349–71
[16] Larsén X G, Larsen S E, Petersen E L and Mikkelsen T K 2019 *Boundary-Layer Meteorology* **171** 191–212
[17] Rose S and Apt J 2012 *Wind Energy* **15** 699–715
[18] Larsén X G, Vincent C and Larsen S 2013 *Quarterly Journal of the Royal Meteorological Society* **139** 685–700
[19] Mikkelsen T, Larsen S E, Jørgensen H E, Astrup P and Larsén X G 2017 *Physica Scripta* **92** 124002
[20] McFarlane A, Veers P and Schluter L 1994 Simulating high-frequency wind for long durations *Thirteenth ASME Wind Energy Symposium* (New Orleans, LA)
[21] Larsén X G, Larsen S E, Petersen E L and Mikkelsen T K 2021 *Boundary-Layer Meteorology* **178** 415–34
[22] Olauson J, Bergkvist M and Rydén J 2017 *Wind Energy* **20** 973–85
[23] Schwarz C M, Ehrich S and Peinke J 2019 *Wind Energy Science* **4** 581–594 URL `https://wes.copernicus.org/articles/4/581/2019/`
[24] Berg J, Natarajan A, Mann J and Patton E G 2016 *Wind Energy* **19** 1975–89